Beyond-mean-field boson-fermion model for odd-mass nuclei

K. Nomura, T. Nikšić, and D. Vretenar

Physics Department, Faculty of Science, University of Zagreb, 10000 Zagreb, Croatia
(Received 7 March 2016; revised manuscript received 11 April 2016; published 2 May 2016)

A novel method for calculating spectroscopic properties of medium-mass and heavy atomic nuclei with an odd number of nucleons is introduced, based on the framework of nuclear energy density functional theory and the particle-core coupling scheme. The deformation energy surface of the even-even core, as well as the spherical single-particle energies and occupation probabilities of the odd particle(s), are obtained in a self-consistent mean-field calculation determined by the choice of the energy density functional and pairing interaction. This method uniquely determines the parameters of the Hamiltonian of the boson core, and only the strength of the particle-core coupling is specifically adjusted to selected data for a particular nucleus. The approach is illustrated in a systematic study of low-energy excitation spectra and transition rates of axially deformed odd-mass Eu isotopes.

I. INTRODUCTION

As in many other quantum systems, the interplay between single-particle and collective degrees of freedom plays a crucial role in the physics of atomic nuclei [1–3]. This is apparent especially in systems with an odd number of protons Z and/or neutrons N. At low energies in nuclei with even Z and N, nucleons are coupled pairwise and this manifests in low-lying rotational and vibrational collective excitations [1]. Many nuclear models have successfully been applied in studies of the structure of even-even nuclei [1–5]. The situation is, however, more complicated in nuclei with odd Z and/or N, because one has to consider unpaired fermions explicitly and treat the single-particle and collective degrees of freedom on the same level [1,6]. Although most nuclear species have an odd Z and/or N, microscopic studies of their structure have not been pursued as extensively as in the case of even-even systems, especially for medium-heavy and heavy nuclei.

Nuclear density functional theory (DFT) provides a reliable global microscopic approach to many structure phenomena [7–10]. The basic implementation of the energy density functional (EDF) framework is in terms of self-consistent mean-field (SCMF) methods, in which an EDF is constructed as a functional of one-body nucleon density matrices that correspond to a single product state. The static nuclear mean field is characterized by the breaking of symmetries of the underlying Hamiltonian—translational, rotational, and particle number—and, therefore, includes important static correlations, e.g., deformations and pairing. To calculate spectroscopic properties, such as excitation spectra and transition rates, the mean-field approach has to be extended to include collective correlations that arise from symmetry restoration and fluctuations around mean-field minima. Collective correlations are taken into account through restoration of broken symmetries and configuration mixing of symmetry-breaking product states using, for instance, the generator coordinate method (GCM) [2].

GCM configuration mixing of angular-momentum and particle-number projected states based on EDFs or effective interactions has become a standard tool for nuclear structure studies of even-even nuclei. However, considerable challenges are encountered when extending this method to odd-mass systems. In fact, it is only recently that such a consistent extension, where the generator coordinate space is built from self-consistently blocked one-quasiparticle Hartree-Fock-Bogoliubov (HFB) states, has been reported in Ref. [11]. Even though this is a very promising approach to a systematic description of odd-mass nuclei, the fact that several blocked states have to be considered at each deformation, as well as the explicit breaking of time-reversal symmetry, presents significant difficulties in realistic applications, especially for heavy nuclei.

A wealth of new data on spectroscopic properties of odd-A nuclei in recent years has led to a renewed interest in particle-vibration coupling (PVC) approaches [1] that explicitly consider the polarization of a nucleus by the odd particle. A number of PVC models of various levels of refinement and self-consistency have been developed [12–19] and applied to studies of structure phenomena. In this work we present an approach based on nuclear DFT and the particle-core coupling scheme [1,6]. It is an extension of a method introduced in Ref. [20] for determining the Hamiltonian of the interacting boson model (IBM) [5], starting with an EDF-based SCMF calculation of deformation energy surfaces. By mapping a deformation constrained energy surface onto the equivalent Hamiltonian of the IBM, that is, onto the energy expectation value in the boson condensate state, the Hamiltonian parameters are determined. The resulting IBM Hamiltonian is used to calculate excitation spectra and transition rates. For an odd-mass nucleus this method is here applied to the even-even core; that is, the even-even core is described in terms of boson degrees of freedom, and only the fermion degrees of freedom of the odd unpaired particle(s) are treated explicitly. By extending the method of Ref. [20] to systems with odd N and/or Z, it becomes equivalent to the well known phenomenological interacting boson-fermion model (IBFM) [21,22]. The advantage of the present approach is that, except for the strength parameter(s) of the boson-fermion coupling, all parameters of the model Hamiltonian are determined by the choice of the (microscopic) energy density functional and pairing interaction. At the cost of having to adjust the

boson-fermion coupling strength to data, we are able to include all states in a major shell in the fermion space, and extend the applicability of the approach to arbitrary heavy odd N and/or Z nuclei.

In Sec. II we describe the method that will be used to determine the boson-core and boson-fermion Hamiltonians, and compare the resulting parameters with those of previous phenomenological calculation in Ref. [23]. Section III presents model results for spectroscopic properties, that is, excitation spectra and electromagnetic transitions and moments. Section IV contains a short summary and concluding remarks.

II. THEORETICAL FRAMEWORK

The model Hamiltonian for an odd-mass nucleus contains a term that corresponds to the even-even (boson) core $\hat{H}_B$, a single-particle Hamiltonian that describes the unpaired nucleon(s) $\hat{H}_F$, and a term that describes the interaction between bosons and fermions $\hat{H}_{BF}$:

$$\hat{H} = \hat{H}_B + \hat{H}_F + \hat{H}_{BF}. \tag{1}$$

The assumption is that the Hamiltonian conserves separately the number of bosons N_B and the number of fermions N_F. Here we will only consider the simplest case with $N_F = 1$. For low-energy states, the dominant components in the boson space are the s (spin 0^+) and d (spin 2^+) bosons [24]. The
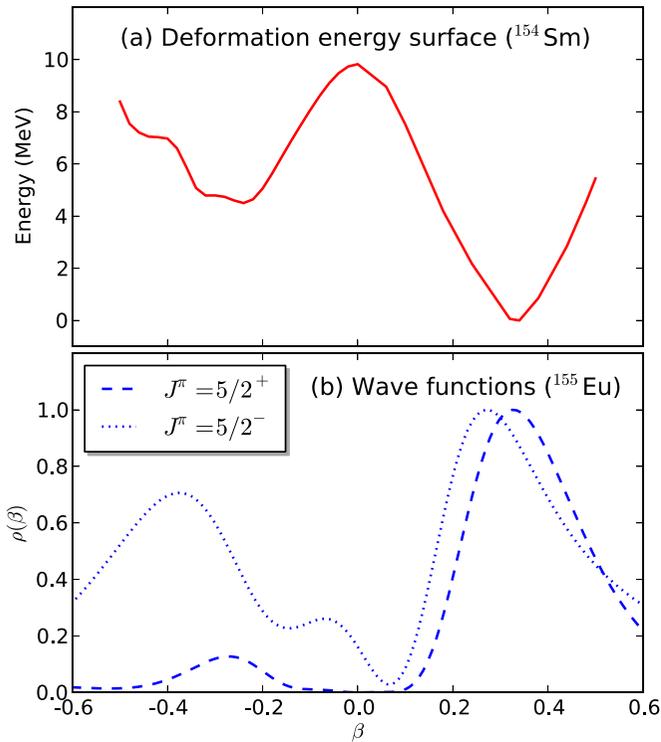
N	ϵ_d	κ	κ'	χ	$\epsilon_{d\,5/2}$	$\epsilon_{d\,3/2}$	$\epsilon_{s\,1/2}$
88	0.46	−0.079	−0.017	−0.55	3.14	5.04	5.74
90	0.29	−0.079	−0.021	−0.55	3.24	5.11	5.88
92	0.13	−0.079	−0.022	−0.55	3.32	5.14	5.98

number of bosons equals the number of valence (spherical open-shell) proton and neutron pairs (particle or hole pairs). Since in the present study the model will be applied to axially deformed rotational nuclei, for the boson Hamiltonian $\hat{H}_B$ we employ the standard form [5]:

$$\hat{H}_B = \epsilon_d \hat{n}_d + \kappa \hat{Q}_B \cdot \hat{Q}_B + \kappa' \hat{L} \cdot \hat{L}, \tag{2}$$

with the d-boson number operator $\hat{n}_d = d^\dagger \cdot \tilde{d}$, the quadrupole operator $\hat{Q}_B = s^\dagger \tilde{d} + d^\dagger \tilde{s} + \chi [d^\dagger \times \tilde{d}]^{(2)}$, and the angular momentum operator $\hat{L} = \sqrt{10}[d^\dagger \times \tilde{d}]^{(1)}$. ϵ_d, κ, κ', and χ are parameters that will be determined by a DFT-based SCMF calculation. The fermion Hamiltonian for a single nucleon reads $\hat{H}_F = \sum_j \epsilon_j [a_j^\dagger \times \tilde{a}_j]^{(0)}$, with ϵ_j the single-particle

FIG. 1. (a) Projection of the RHB deformation energy surface along the β axis for ^{155}Eu, plotted with respect to the minimum. The calculation is based on the relativistic density functional DD-PC1 and a separable pairing force of finite range. (b) Distribution $\rho(\beta)$ of the wave functions for the lowest-lying positive-parity ($J^\pi = 5/2^+$) and negative-parity ($J^\pi = 5/2^-$) states of ^{155}Eu (see the text for details).
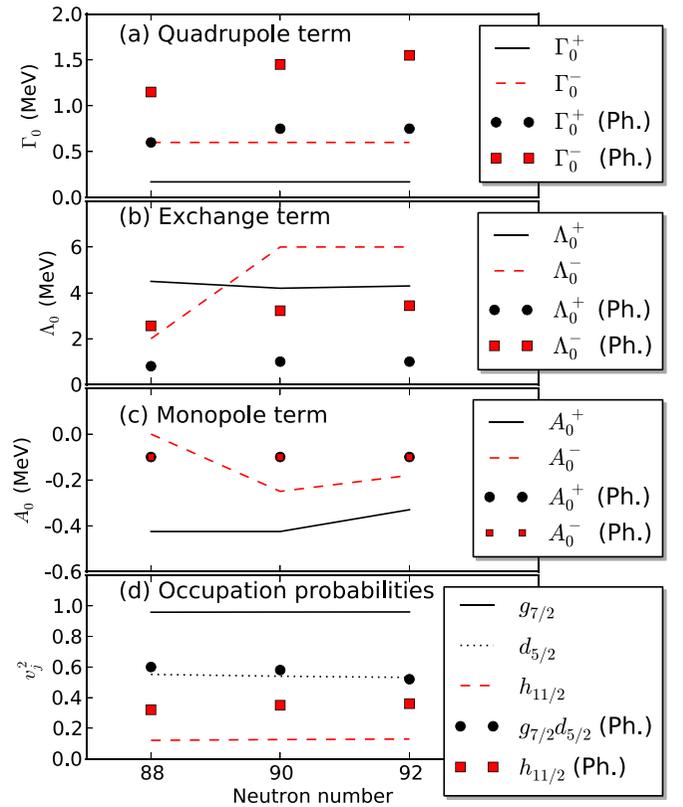

FIG. 2. Values of the parameters $\Gamma_0^\pm$ (a), $\Lambda_0^\pm$ (b), and $A_0^\pm$ (c) for positive- and negative-parity states, and the occupation probabilities v^2 of the spherical orbitals $1g_{7/2}$, $2d_{5/2}$, and $1h_{11/2}$ (d). The corresponding values used in Ref. [23], denoted by "Ph.", are shown for comparison. In Ref. [23] identical occupation probabilities were used for the orbitals $1f_{7/2}$ and $2d_{5/2}$.

energy of the spherical orbital j. For the particle-core coupling $\hat{H}_{BF}$ we use the simplest form [21,22]:

$$
\begin{aligned}
\hat{H}_{BF} = &\sum_{jj'} \Gamma_{jj'} \hat{Q}_B \cdot [a_j^\dagger \times \tilde{a}_{j'}]^{(2)} \\
&+ \sum_{jj'j''} \Lambda_{jj'}^{j''} : [[d^\dagger \times \tilde{a}_j]^{(j'')} \times [a_{j'}^\dagger \times \tilde{d}]^{(j'')}]^{(0)} : \\
&+ \sum_j A_j [a^\dagger \times \tilde{a}_j]^{(0)} \hat{n}_d,
\end{aligned}
\tag{3}
$$

where the first and second terms are referred to as the quadrupole and exchange interaction, respectively. The former describes the quadrupole boson-fermion interaction, whereas the latter takes into account the fact that bosons are fermion pairs and its inclusion is essential for a detailed reproduction of low-energy spectra and electromagnetic transition probabilities. $\hat{Q}_B$ is the same boson quadrupole operator as in $\hat{H}_B$, and $: (\cdots) :$ indicates normal ordering. The strength parameters $\Gamma_{jj'}$ and $\Lambda_{jj'}^{j''}$ can be rewritten, by use of the generalized seniority scheme, in the following j-dependent forms [25]:

$$
\Gamma_{jj'} = \Gamma_0 \gamma_{jj'},
\tag{4}
$$

$$
\Lambda_{jj'}^{j''} = -2\Lambda_0 \sqrt{\frac{5}{2j''+1}} \beta_{jj''} \beta_{j'j''},
\tag{5}
$$

where $\gamma_{jj'} = (u_j u_{j'} - v_j v_{j'}) Q_{jj'}$ and $\beta_{jj'} = (u_j v_{j'} + v_j u_{j'}) Q_{jj'}$, and the matrix element of the quadrupole operator in the single-particle basis $Q_{jj'} = \langle j || Y^{(2)} || j' \rangle$. The factors u_j and v_j denote the occupation probabilities of the orbit j, and satisfy $u_j^2 + v_j^2 = 1$. The last term in Eq. (3) denotes the monopole term. A_j can be parametrized as $A_j = -\sqrt{2j+1} A_0$ with A_0

denoting the strength parameter [23]. The effect of this term is to compress or expand the single-nucleon energy levels [21].

As an illustrative application of the method, we consider the case of a single nucleon coupled to an axially symmetric rotor: the low-energy spectra of the isotopes ^{151,153,155}Eu. These nuclei were extensively investigated in the IBFM calculation of Ref. [23] and, therefore, one can directly compare the present results with those obtained in a purely phenomenological approach. The corresponding even-even core nuclei ^{150,152,154}Sm present excellent examples of axially deformed rotors [5]. The number of bosons equals the number of nucleon pairs outside the doubly magic core ^{132}Sn, that is, 9, 10, and 11 for ^{151,153,155}Eu, respectively.

In the first step of the construction of the boson-fermion Hamiltonian $\hat{H}$ in Eq. (1), the parameters for the even-even core $\hat{H}_B$ Eq. (2) are determined. To this aim we employ the procedure developed in Refs. [20,26]: based on a specific choice for a nuclear EDF, the constrained SCMF calculation determines the microscopic deformation energy surface as function of the polar deformation parameters β and γ [1]. This energy surface is mapped onto the corresponding expectation value of the boson Hamiltonian in the intrinsic (coherent) state [27] of the interacting boson system, and this mapping completely determines the parameters of $\hat{H}_B$. Only the strength parameter κ' for the $\hat{L} \cdot \hat{L}$ term is determined separately so that the cranking moment of inertia in the IBM intrinsic state becomes equal to the Inglis-Belyaev moment of inertia $\mathcal{I}$ obtained from the self-consistent cranking calculation at the mean-field minimum [26]. Here $\mathcal{I}$ is increased by 30%, taking into the fact that the Inglis-Belyaev formula gives significantly smaller moment of inertia than the empirical values.

As an illustration, Fig. 1(a) displays the projection of the energy map of ^{154}Sm along the axis of β deformation,
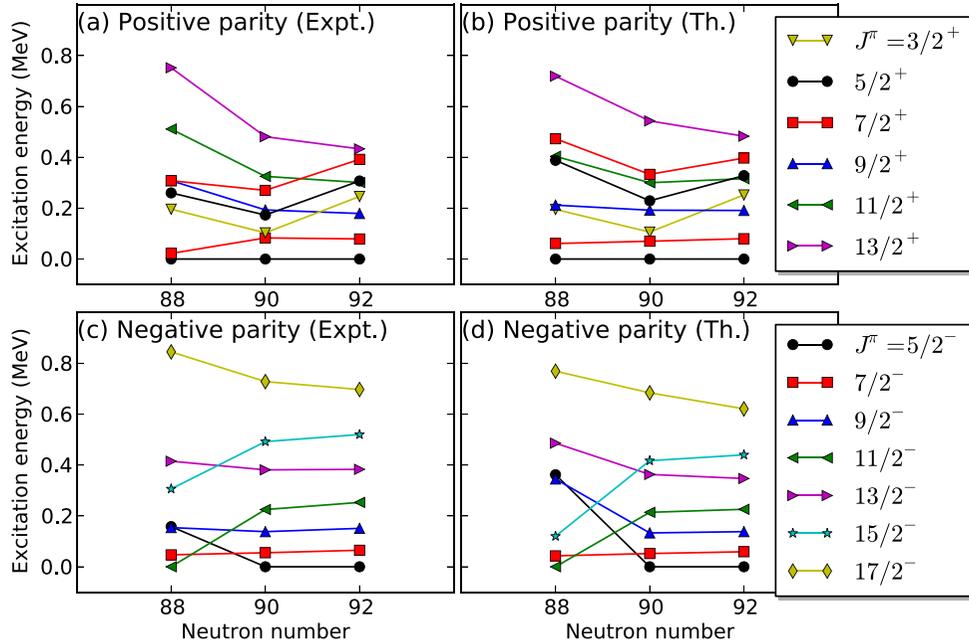

FIG. 3. The calculated low-energy positive- and negative-parity levels of ^{151,153,155}Eu plotted in comparison with their experimental counterparts [31].

obtained from the constrained self-consistent relativistic Hartree-Bogoliubov (RHB) calculation based on the energy density functional DD-PC1 [28] and a separable pairing force of finite range [29]. One notices a pronounced prolate equilibrium minimum at $\beta_{\min} \approx 0.34$. The corresponding parameters $\epsilon_d, \kappa, \kappa'$, and χ of $\hat{H}_B$, determined by the mapping of the microscopic energy surface, are summarized in Table I.

For the fermion valence space we include all the spherical single-particle orbits in the proton major shell $Z = 50$–82: $1g_{7/2}, 2d_{5/2}, 2d_{3/2}$, and $3s_{1/2}$ for positive-parity, and $1h_{11/2}$ for negative parity, with single-particle (canonical) energies and occupation probabilities determined by the self-consistent RHB calculation constrained at zero deformation. It remains then to adjust the three strength parameters of the boson-fermion interaction Hamiltonian $\hat{H}_{BF}$. Γ_0, Λ_0, and A_0 are the only parameters that are fitted to data, separately for positive- and negative-parity states. For each nucleus, the optimal values for the strength parameters are chosen so as to reproduce the energies of the first excited state and of the band head of the second-lowest band. We include the monopole term only for $2d_{5/2}$ and $1h_{11/2}$ orbitals so as to improve the description of the band head of the second-lowest band.

The resulting total boson-fermion Hamiltonian $\hat{H}$ is diagonalized numerically in the spherical basis $|j, L, \alpha, J\rangle$, where α is a generic notation for a set of quantum numbers n_d, υ, n_Δ that distinguish states with the same boson angular momentum L [5], and J is the total angular momentum of the Bose-Fermi system $(|L - j| \leqslant J \leqslant L + j)$.

To illustrate the method, we display in Fig. 1(b) the distribution $\rho(\beta)$ of the wave functions for the lowest positive- and negative-parity states of ^{155}Eu as functions of the axial deformation β. The function $\rho(\beta)$ is computed by taking the overlap between the eigenstate of the IBFM Hamiltonian and the projected intrinsic state of the coupled boson-fermion system expanded in terms of the basis $|j, L, \alpha, J\rangle$ [30]. Starting from the spherical single-proton states, as a result of the interaction $\hat{H}_{BF}$ between the unpaired proton and the deformed boson core, the distributions of wave functions for both states $J^\pi = 5/2_1^+$ and $5/2_1^-$ display peaks close to the minimum of the energy surface of the even-even core ^{154}Sm. The additional peaks at the corresponding negative values of β ($\gamma = 60°$) arise because the energy surface exhibits a parabolic dependence on γ [cf. panel (a) of Fig. 1].

In Fig. 2 we plot the strengths parameters Γ_0 (a), Λ_0 (b), A_0 (c), and the RHB occupation probabilities υ_j^2 of the spherical orbits $1g_{7/2}, 2d_{5/2}$, and $1h_{11/2}$ (d). The values used in the fully phenomenological calculation of Ref. [23] are also included for comparison. One notices that, for states of both parities, the values of Γ_0, Λ_0, and A_0 used in the present calculation are significantly different from the ones of Ref. [23]. The difference most likely results from the occupation probabilities and energy spacing between the $1g_{7/2}$ and $2d_{5/2}$ single-particle levels: from Fig. 2(d), $\upsilon_{g7/2}^2 \approx 0.96$, $\upsilon_{d5/2}^2 \approx 0.55$ and $\upsilon_{h11/2}^2 \approx 0.13$ in the present study, whereas $\upsilon_{g7/2}^2 = \upsilon_{d5/2}^2 \approx 0.5$–$0.6$ and $\upsilon_{h11/2}^2 \approx 0.35$ in [23]. From Table I, we note that $|\epsilon_{g7/2} - \epsilon_{d5/2}| \approx 3$ MeV, in contrast to <0.5 MeV in Ref. [23]. Nevertheless, in both studies Γ_0 and Λ_0 display a smooth variation with neutron number. Another

difference is that in Ref. [23] the monopole boson-fermion interaction with a constant strength parameter $A_0 = -0.1$ MeV was included in the Hamiltonian for all orbitals, whereas the monopole term is used only for $2d_{5/2}$ and $1h_{11/2}$ orbitals and varies smoothly with neutron number in the present calculation.

III. ODD-*A* EUROPIUM ISOTOPES

Figure 3 compares the calculated low-energy positive- and negative-parity levels of ^{151,153,155}Eu to available data [31]. For the positive-parity states [Figs. 3(a) and 3(b)], the $5/2_1^+$ state is the ground state in all three nuclei. For ^{153,155}Eu the levels above the ground state, that is, $7/2_1^+, 9/2_1^+, 11/2_1^+$, and $13/2_1^+$, form a rotational band with excitation energies proportional to $J(J + 1)$ (cf. also Figs. 5 and 6). ^{151}Eu differs in structure from ^{153,155}Eu by the fact that its $7/2_1^+$ state is low in energy and close to the $5/2_1^+$ ground state. Indeed, its boson core ^{150}Sm is rather close to the transitional region between rotational and vibrational nuclei, whereas ^{153,155}Eu are prolate
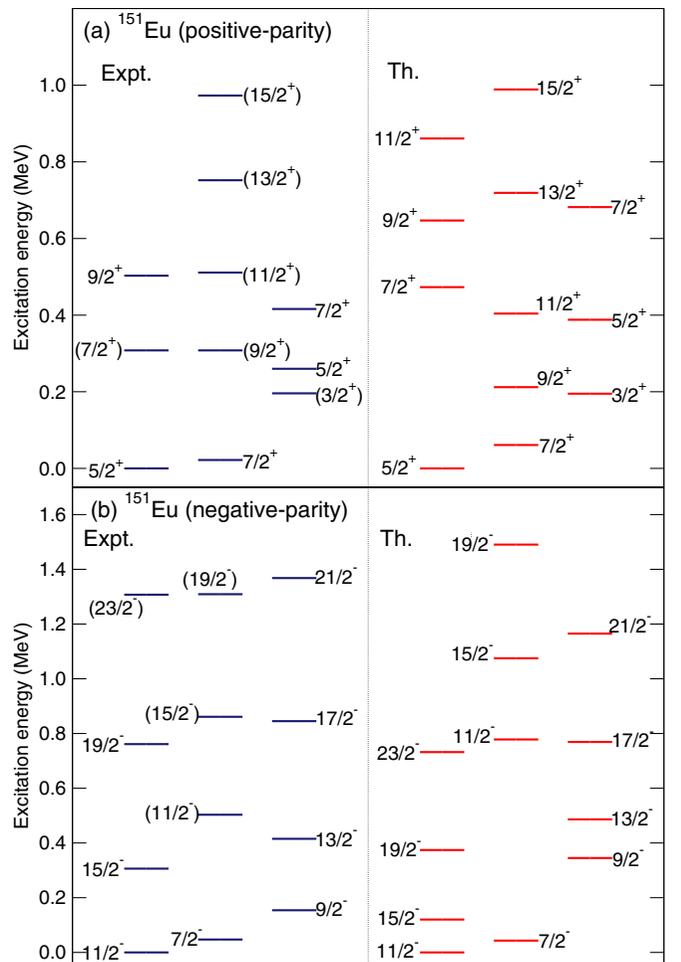

FIG. 4. Detailed comparison of the calculated low-energy levels of ^{151}Eu with available data [31]. The excitation energies for the negative-parity states are shown relative to the lowest state. Note that the experimental states in parentheses denote tentative assignments.

deformed rotors. Considering that only three free parameters are adjusted to data, the calculation quantitatively reproduces the experimental systematics, except perhaps for the excitation energy of the $7/2_2^+$ level in ^{151}Eu. The $3/2_2^+$ state is supposed to be the band head of the excited band, followed by the levels $5/2_2^+$ and $7/2_2^+$. For the negative-parity states in Figs. 3(c) and 3(d), the model results agree with the empirical rotational-like level structure in ^{153,155}Eu. A significant structural change is obtained in ^{151}Eu, in which the $11/2^-$ level becomes the ground state.

We emphasize the fact that the model can describe not only systematic trends of low-lying levels, but also details of excitation spectra and decay patterns in individual nuclei. Figures 4, 5, and 6 display the comparison between theoretical and experimental low-energy levels for the positive and negative-parity states of ^{151,153,155}Eu, respectively. The levels are grouped into bands according to the dominant decay pattern. One notes that, overall, the theoretical results are in good agreement with experiment, particularly for the more deformed ^{153,155}Eu. The present results reproduce data on the same level of accuracy as the fully phenomenological approach of Ref. [23].
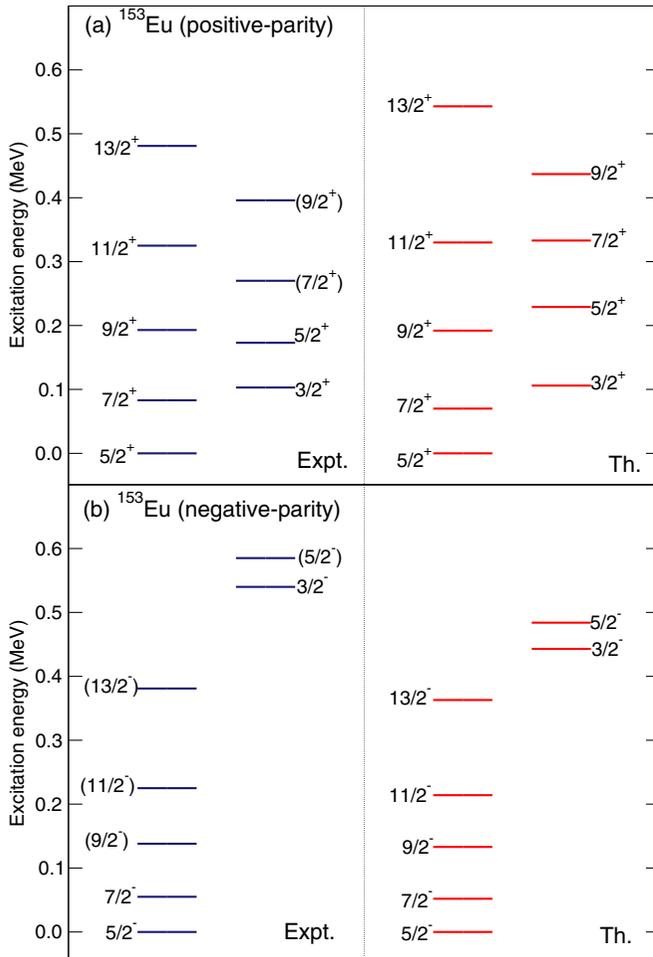

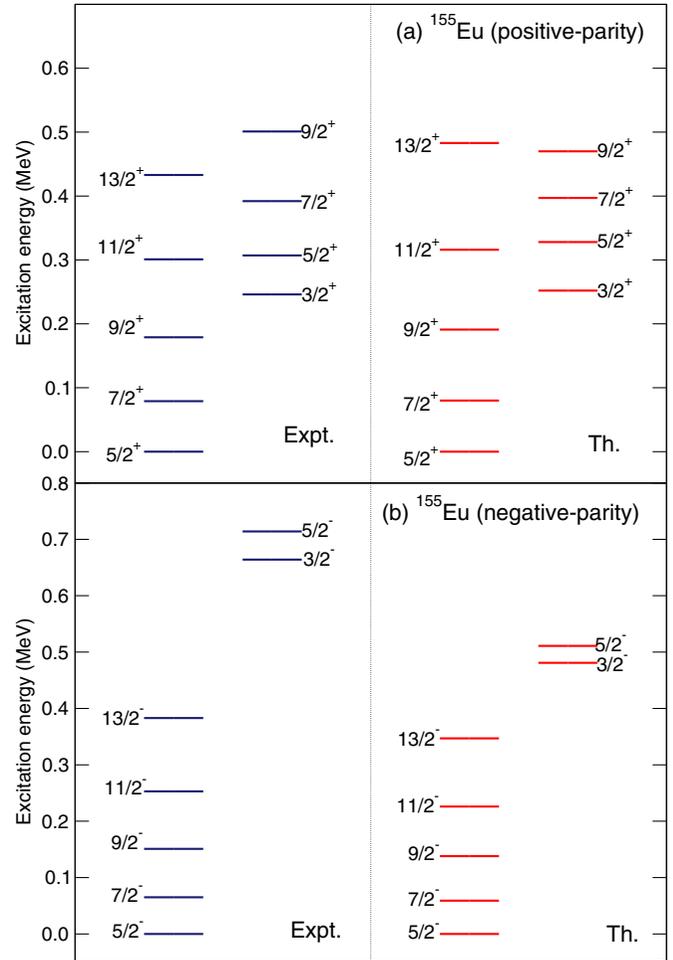FIG. 5. Same as in the caption to Fig. 4, but for the isotope ^{153}Eu.

FIG. 6. Same as the caption to Fig. 4, but for ^{155}Eu.

For ^{151}Eu it was suggested in Ref. [23] that the positive-parity $5/2_1^+$ and $7/2_1^+$ states correspond to the $2d_{5/2}$ and $1g_{7/2}$ single-particle states, and become the band heads of the bands $(5/2_1^+, 7/2_2^+, 9/2_2^+, \ldots)$ and $(7/2_1^+, 9/2_1^+, 11/2_1^+, \ldots)$, respectively. In the present study, in contrast, the levels that belong to both bands, built on $5/2_1^+$ and $7/2_1^+$ states, are predominantly based on the $1g_{7/2}$ configuration. For the negative-parity states of ^{151}Eu in Fig. 4(b) our calculation predicts that the three bands based on $11/2_1^-$, $7/2_1^-$, and $9/2_1^-$ follow the $\Delta J = 2$ systematics of states decoupled from the deformation of the core. Figures 5 and 6 show that the band structures of ^{153}Eu and ^{155}Eu are very similar. In both nuclei the two positive-parity bands built on the states $J^\pi = 5/2^+$ and $3/2^+$ are assigned to the $K^\pi = 5/2^+$ and $K^\pi = 3/2^+$ rotational bands, respectively. The level energies of these $J(J+1)$ rotational bands exhibit the strong-coupling $\Delta J = 1$ systematics. The positive-parity bands based on $5/2_1^+$ and $3/2_1^+$ predominantly correspond to the $1g_{7/2}$ and $2d_{5/2}$ proton configurations, respectively, with significant mixing of the two configurations. The similarity between band structures in ^{153}Eu and ^{155}Eu is also evident for the negative-parity bands based on the $1h_{11/2}$ spherical orbital.

TABLE II. The calculated reduced $E2$ (in Weisskopf units) and $M1$ (in μ_N^2) transition probabilities for low-lying states, and spectroscopic quadrupole moments $Q(J^\pi)$ (in b) and magnetic moments $\mu(J^\pi)$ (in μ_N) for ^{151,153,155}Eu, compared to available experimental values [31–35].

	^{151}Eu		^{153}Eu		^{155}Eu	
	Th.	Expt.	Th.	Expt.	Th.	Expt.
$B(E2; 3/2_1^+ \to 5/2_1^+)$	18	22(12)	40	1.4(5)	4.3	0.47(9)
$B(E2; 3/2_1^+ \to 7/2_1^+)$	4.0	2.4(4)	22	1.9(4)	3.6	0.73(6)
$B(E2; 5/2_2^+ \to 3/2_1^+)$	86		210	154(82)	281	
$B(E2; 5/2_2^+ \to 5/2_1^+)$	10		34	0.9(4)	3.9	
$B(E2; 5/2_2^+ \to 7/2_1^+)$	0.8		0.8	2.8(1.7)	0.012	
$B(E2; 7/2_1^+ \to 5/2_1^+)$	57	8.1(9)	190	300(21)	267	
$B(E2; 7/2_2^+ \to 5/2_1^+)$	26		7.2	0.53(7)	9.8	
$B(E2; 7/2_2^+ \to 7/2_1^+)$	34	<80	47	4(4)	24	
$B(E2; 9/2_1^+ \to 5/2_1^+)$	10		51	97(8)	68	
$B(E2; 9/2_1^+ \to 7/2_1^+)$	87		198	179(21)	246	
$B(E2; 3/2_1^- \to 5/2_1^-)$	11		20		0.5	
$B(E2; 7/2_1^- \to 5/2_1^-)$	38		241		266	
$B(E2; 9/2_1^- \to 7/2_1^-)$	6.7	>70	197		222	
$B(M1; 3/2_1^+ \to 5/2_1^+)$	0.0098	0.0078(16)	0.016	0.0034(1)	0.000072	0.00098(9)
$B(M1; 5/2_2^+ \to 3/2_1^+)$	0.167		0.11	0.22(2)	0.120	
$B(M1; 5/2_2^+ \to 5/2_1^+)$	0.00024		0.00055	0.00016(4)	0.00030	
$B(M1; 5/2_2^+ \to 7/2_1^+)$	0.0077		0.012	0.0030(3)	0.0011	
$B(M1; 7/2_1^+ \to 5/2_1^+)$	0.0060	0.0083(4)	0.020	0.011(1)	0.021	
$B(M1; 7/2_2^+ \to 5/2_1^+)$	0.089	0.20(5)	0.048	4.6×10^{-5}(4)	0.046	
$B(M1; 7/2_2^+ \to 7/2_1^+)$	0.020	0.015(5)	0.018	0.00106(6)	0.011	
$B(M1; 9/2_1^+ \to 7/2_1^+)$	0.016		0.034	0.016(1)	0.033	
$B(M1; 3/2_1^- \to 5/2_1^-)$	1.73		2.49		2.75	
$B(M1; 7/2_1^- \to 5/2_1^-)$	0.26		0.014		0.14	
$B(M1; 9/2_1^- \to 7/2_1^-)$	0.55		0.039		0.20	
$Q(3/2_1^+)$	+0.70		+1.14	1.254(13)	+1.27	
$Q(5/2_1^+)$	+1.16	+0.903(10)	+1.79	+2.28(9)	+2.26	+2.49(2)
$Q(7/2_1^+)$	+0.79	1.28(2)	+0.63	+0.44(2)	+0.63	
$\mu(3/2_1^+)$	+1.22		+1.25	+2.048	+1.22	
$\mu(5/2_1^+)$	+1.53	+3.4717(6)	+1.54	+1.53	+1.52	+1.52
$\mu(7/2_1^+)$	+2.02	+2.591(2)	+1.93	+1.81(6)	+1.86	
$\mu(5/2_1^-)$	+5.52		+3.05	+3.22(23)	+2.96	+9.6(10)

The relevant decay modes are the electric quadrupole ($E2$) and magnetic dipole ($M1$) transitions. The corresponding operator $T^{(E2)} = e_B \hat{Q}_B + e_F \hat{Q}_F$, with $\hat{Q}_F = -\sum_{jj'} \gamma_{jj'} [a_j^\dagger \times \tilde{a}_{j'}]^{(2)}/\sqrt{5}$, and e_B and e_F denote the effective charges. e^B is adjusted to reproduce the experimental $B(E2; 2_1^+ \to 0_1^+)$ value for the boson core nucleus, and the constant value $e_F = 1.0$ eb is used for the unpaired proton. The magnetic dipole operator $T^{(M1)} = \sqrt{3/4\pi}(g^B \hat{L} + \sum_j g_j^F \hat{j})$, where $\hat{j}$ is the fermion angular momentum operator, and g^B and g_j^F are the boson and fermion g factors, respectively. g^B is adjusted to the experimental magnetic moment of the 2_1^+ state of the boson core, $g^B = \mu(2_1^+)/2$, and the Schmidt values are used for g_j^F, with the spin g factor quenched by 30%. Data are available for $E2$ and $M1$ transitions between low-lying states of positive-parity bands.

Table II collects the results for the $E2$ and $M1$ transition strengths, spectroscopic quadrupole moments, and magnetic moments. In general, with only a few exceptions, the present study reproduces available data [31–33], and is consistent with the results obtained in Ref. [23]. In this calculation rather strong in-band $E2$ and $M1$ transitions for the bands built on the $5/2_1^+$ and $3/2_1^+$ states are predicted for ^{153,155}Eu. Because of the pronounced mixing between the $2d_{5/2}$ and $1g_{7/2}$ configurations, the calculated interband transitions are rather large in all considered isotopes, and overestimate the data such as, the $7/2_1^+ \to 5/2_1^+$ and $3/2_1^+ \to 5/2_1^+$ $E2$ transitions in ^{151}Eu and ^{153}Eu, respectively. Note that, except for ^{153}Eu, the data on $B(E2)$ and $B(M1)$ values are rather scarce. The calculated spectroscopic quadrupole and magnetic moments for low-lying states are in good agreement with the available experimental values [31,35].

IV. SUMMARY

In conclusion, we have introduced an advanced method for calculating spectroscopic properties of medium-mass and heavy nuclei with odd N and/or Z. The IBFM Hamiltonian used to describe the coupled system of the unpaired particle(s) plus boson core is based on the microscopic framework of nuclear energy density functional theory. The deformation energy surface of the even-even core, as well as the spherical single-particle energies and occupation probabilities of the odd particle(s), are obtained in a SCMF calculation determined by the choice of the energy density functional and pairing interaction. Only the strength parameter(s) of the boson-fermion interaction Hamiltonian are specifically adjusted to data for each nucleus. As an illustrative example, the low-energy excitation spectra and transition rates of $^{151-155}$Eu have been analyzed, and a very good agreement with data has been obtained. The microscopic approach in which the even-even core is described in terms of boson degrees of freedom, and only the fermion degrees of freedom of the unpaired particle(s) are treated explicitly, enables an accurate, computationally feasible, and systematic description of a wealth of new data on isotopes with an odd number of protons and/or neutrons.

[1] A. Bohr and B. M. Mottelsson, *Nuclear Structure*, Vol. 2 (Benjamin, New York, 1975).

[2] P. Ring and P. Schuck, *The Nuclear Many-Body Problem* (Springer-Verlag, Berlin, 1980).

[3] R. F. Casten, *Nuclear Structure from a Simple Perspective* (Oxford University Press, Oxford, 1990).

[4] E. Caurier, G. Martínez-Pinedo, F. Nowacki, A. Poves, and A. P. Zuker, Rev. Mod. Phys. **77**, 427 (2005).

[5] F. Iachello and A. Arima, *The Interacting Boson Model* (Cambridge University Press, Cambridge, 1987).

[6] A. Bohr, K. Dan. Vidensk. Selsk. Mat. Fys. Medd. **27**, 16 (1953).

[7] M. Bender, P.-H. Heenen, and P.-G. Reinhard, Rev. Mod. Phys. **75**, 121 (2003).

[8] D. Vretenar, A. V. Afanasjev, G. Lalazissis, and P. Ring, Phys. Rep. **409**, 101 (2005).

[9] *Extended Density Functionals in Nuclear Structure Physics*, edited by G. Lalazissis, P. Ring, and D. Vretenar, Lecture Notes in Physics Vol. 641 (Springer, Berlin, 2004).

[10] J. Stone and P.-G. Reinhard, Prog. Part. Nucl. Phys. **58**, 587 (2007).

[11] B. Bally, B. Avez, M. Bender, and P.-H. Heenen, Phys. Rev. Lett. **113**, 162501 (2014).

[12] E. Litvinova, P. Ring, and V. Tselyaev, Phys. Rev. C **75**, 064308 (2007).

[13] K. Yoshida, Phys. Rev. C **79**, 054303 (2009).

[14] G. Colò, H. Sagawa, and P. F. Bortignon, Phys. Rev. C **82**, 064307 (2010).

[15] E. V. Litvinova and A. V. Afanasjev, Phys. Rev. C **84**, 014305 (2011).

[16] K. Mizuyama, G. Colò, and E. Vigezzi, Phys. Rev. C **86**, 034318 (2012).

[17] D. Tarpanov, J. Toivanen, J. Dobaczewski, and B. G. Carlsson, Phys. Rev. C **89**, 014307 (2014).

[18] D. Tarpanov, J. Dobaczewski, J. Toivanen, and B. G. Carlsson, Phys. Rev. Lett. **113**, 252501 (2014).

[19] Y. F. Niu, Z. M. Niu, G. Colò, and E. Vigezzi, Phys. Rev. Lett. **114**, 142501 (2015).

[20] K. Nomura, N. Shimizu, and T. Otsuka, Phys. Rev. Lett. **101**, 142501 (2008).

[21] F. Iachello and P. Van Isacker, *The Interacting Boson-Fermion Model* (Cambridge University Press, Cambridge, 1991).

[22] *Interacting Bose-Fermi Systems in Nuclei*, edited by F. Iachello (Springer, New York, 1981).

[23] O. Scholten and N. Blasi, Nucl. Phys. A **380**, 509 (1982).

[24] T. Otsuka, A. Arima, and F. Iachello, Nucl. Phys. A **309**, 1 (1978).

[25] O. Scholten, Prog. Part. Nucl. Phys. **14**, 189 (1985).

[26] K. Nomura, T. Otsuka, N. Shimizu, and L. Guo, Phys. Rev. C **83**, 041302 (2011).

[27] J. N. Ginocchio and M. W. Kirson, Nucl. Phys. A **350**, 31 (1980).

[28] T. Nikšić, D. Vretenar, and P. Ring, Phys. Rev. C **78**, 034318 (2008).

[29] Y. Tian, Z. Y. Ma, and P. Ring, Phys. Lett. B **676**, 44 (2009).

[30] A. Leviatan, Phys. Lett. B **209**, 415 (1988).

[31] Brookhaven National Nuclear Data Center, http://www.nndc.bnl.gov

[32] J. Hess, Nucl. Phys. A **142**, 273 (1970).

[33] C. Gunther and J. Soares, Nucl. Phys. A **257**, 1 (1976).

[34] L. Kroger and C. Reich, Nucl. Data Sheets **15**, 409 (1975).

[35] N. Stone, At. Data Nucl. Data Tables **90**, 75 (2005).